CHAPTER 3

Anomalous and Topological Hall effect in Cu doped Sb_2Te_3 topological insulator

Chapter 3

3.1. Introduction

Finding anomalous [49] and topological Hall effect [17], [50] in topological materials is very promising both from basic research and application point of view. Anomalous Hall effect (AHE) exists due to the magnetic interaction of localized and conduction electrons, whereas topological Hall effect (THE) is a hallmark of topologically nontrivial (chiral) spin textures. Generally, THE is observed in B20 phase materials [51], [52] but the same has also been observed in some other kind of materials [53]–[55]. While this phenomenon can be understood in ferromagnetic materials, recently this has also been reported in antiferromagnetic system [18]. In topologically non-trivial HgTe [13], [56] the THE has already been predicted. However, the existence of THE has been reported in antiferromagnetic GdPtBi [18], the electronic structure of which is similar to that of HgTe.

Moreover, recently, topological insulators (TIs) have attracted a great attention to the scientific community for their interesting physical properties. The surface state in TIs which is conducting unlike insulating bulk state is topologically protected by time reversal symmetry (TRS) due to the strong spin-orbit (SO) coupling [1]. The delocalized topological surface states (TSS) remain unaffected with nonmagnetic doping and their excitation spectrum within the bulk energy gap exhibits the characteristic Dirac dispersion because of this time reversal symmetry.

On the other hand, for the spontaneously TRS broken systems, both spin dependent scattering and the real and momentum space Berry phase [49], [50], [57] contribute to transverse velocity. The former is related to non-coplanar spin textures with finite scalar spin chirality and the latter is observed in TRS broken systems which originate from Berry curvature of the filled bands that is induced by the SO interaction. The magnetic texture

induced AHE is generally associated with finite spin chirality and exhibits anomalous Hall angles ~0.01 (such as $SrFeO_3$ [58] or $Pr_2Ir_2O_7$ [59]). But in ferromagnets intrinsic band structure affects significantly. However, it has been suggested theoretically that non-collinear antiferromagnets may be affected by magnetic texture and strong SOC leading to significant Hall responses [60]. In the present study we have shown the existence of THE in Cu doped Sb_2Te_3 topological insulator.

3.2. Experimental Details

The single crystal of $Sb_{1.90}Cu_{0.10}Te_3$ was grown by using modified Bridgman method, as has already been reported [61]. The obtained crystal was easily cleaved along (*00l*) direction. The chemical state of samples has been analysed by X-ray photoelectron spectrophotometer (XPS) (PHI Versa Probe 5000 II (ULVAC- PHI) using Al Kα radiation. The electrical transport properties were carried out by using physical property measurement system (PPMS, Quantum Design). The magnetic properties were carried out by using magnetic property measurement system (MPMS, Quantum Design).

3.3 Results and Discussion

3.3.1 Experimental Study

In the present investigation, we have focussed the correlation between magnetic structure and strong spin-orbit coupling. We have characterized as grown single crystal sample after cleaving in (*00l*) direction with the help of X-Ray diffraction and Laue diffraction techniques. Hence, the reflections corresponding (*00l*) planes have been observed from XRD as shown in figure 3.1.

Magnetotransport measurements can give a valuable information of the correlation of the conduction electrons to the magnetic ordering. The variation of resistivity as a function

of temperature of $Sb_{1.90}Cu_{0.10}Te_3$ has been measured. It is observed that resistivity value increases with increasing temperature as illustrated in figure 3.2 (a). As displayed in figure 3.2 (b) $Sb_{1.90}Cu_{0.10}Te_3$ shows a large linear MR (nearly 45%) at low temperature but with increase of temperature MR decreases. For a high magnetic field, quantum oscillations were observed at low temperatures.

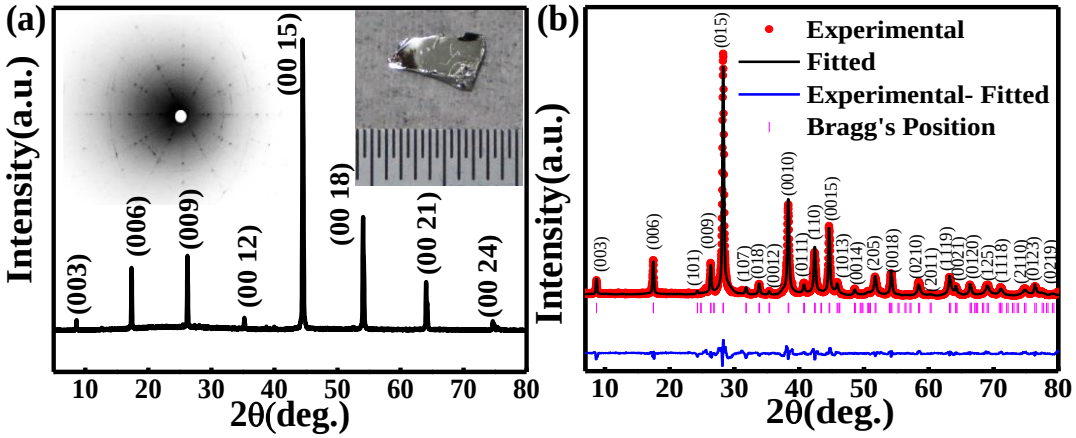

Figure 3.1: (a) XRD pattern for $Sb_{1.90}Cu_{0.10}Te_3$ single crystal sample cleaved along (*00l*) direction. Left Inset: Laue Diffraction pattern, Right Inset: Optical image of the cleaved $Sb_{1.90}Cu_{0.10}Te_3$ single crystal sample. (b) Rietveld refinement of powder XRD for $Sb_{1.90}Cu_{0.10}Te_3$ sample.

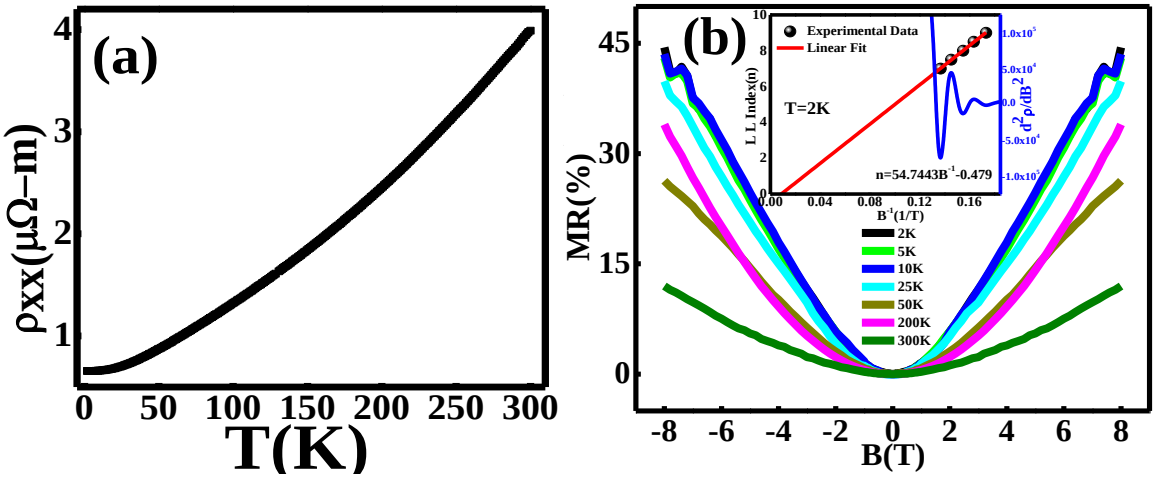

Figure 3.2: (a) The variation of resistivity as a function of temperature (b) MR as a function of magnetic field (B) at different temperatures, Inset: SdH oscillations from the longitudinal resistance and Landau level indexing (Fan Diagram) with inverse magnetic field and linearly fitted curve (red line).

The Landau level Fan diagram obtained from quantum oscillation shows an intercept at ~-0.479 (figure 3.2 (b): inset), indicating that the Dirac fermions dominate the transport properties due to the additional Berry phase π [62].

The variations of magnetization with magnetic field as well as temperature are shown in figure 3.3. We observe that magnetization increases with increasing magnetic field. The magnetic susceptibility (χ) vs. T curve (inset of figure 3.3), is fitted using the following equation

$$\chi = \chi_0 + (D \times T) + C/(T-\theta) \qquad (3.1)$$

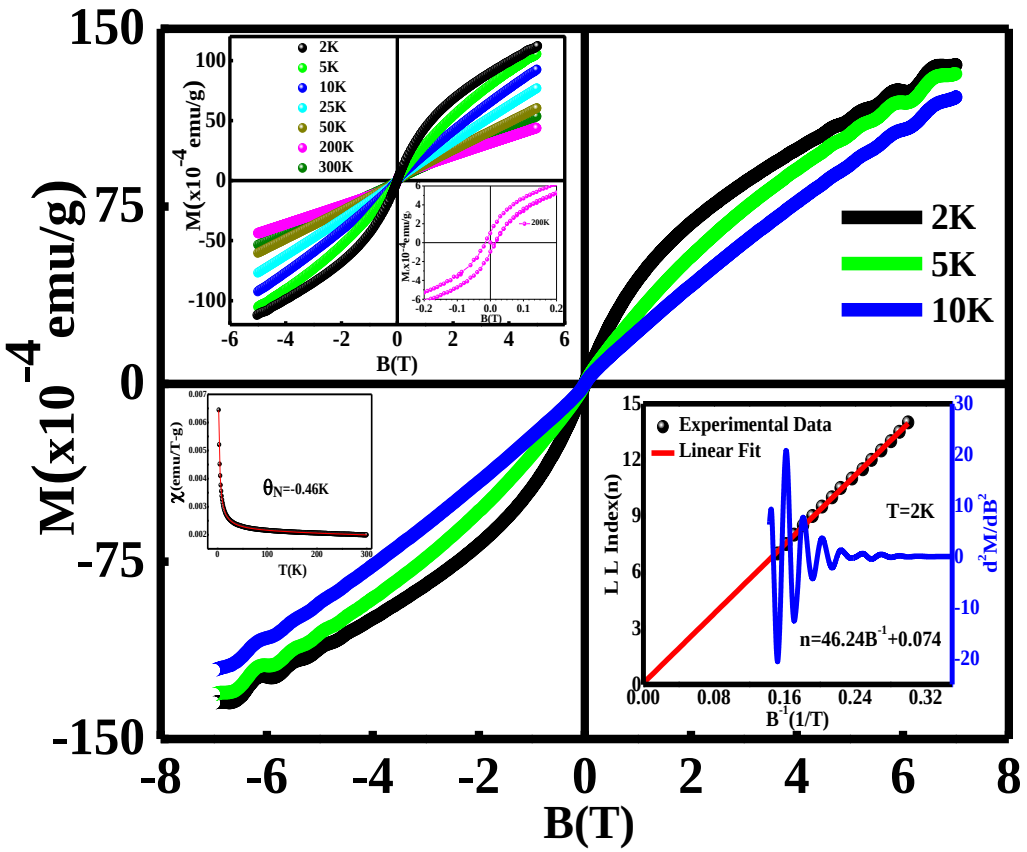

Figure 3.3: Field dependence of magnetization of $Sb_{1.90}Cu_{0.10}Te_3$ at different temperatures, Insets: temperature dependence of magnetization in ZFC mode at an applied magnetic field of 1000 Oe, Magnified view of M vs B curve at 200 K, dHvA oscillations from the magnetization and Landau level indexing (Fan Diagram) with inverse magnetic field and linearly fitted curve (red line).

First two terms in equation (3.1) describe the diamagnetic contribution in magnetic susceptibility whereas third term is indicating the Curie-Weiss expression. Best fit of experimental data gives θ= -0.46K, the negative value of θ indicates the anti-ferromagnetic nature.

For further confirmation of the anti-ferromagnetic ordering, magnetization (M) vs magnetic field (B) measurement is carried out at different temperatures. It is clear from the M vs B curve that M increases with the increase of B. Moreover, no saturation is seen even at the applied field of ±5 T, which is a clear signature of anti-ferromagnetic ordering. Interestingly, nature of curve remains anti-ferromagnetic even at room temperature (i.e. 300 K) (figure 3.3: Inset). Moreover, quantum oscillation (de-Haas-van-Alfen oscillation) is observed at higher field and at low temperature (≤ 10 K). The Fan level diagram (with intercept ~0.074) obtained from this quantum oscillation clearly indicates the bulk contribution in the magnetic origin.

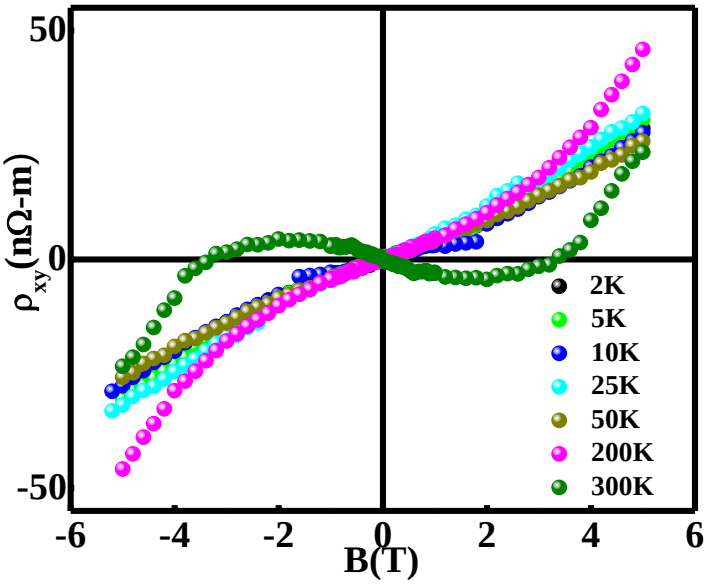

Figure 3.4: Magnetic field dependence of the Hall resistivity of $Sb_{1.90}Cu_{0.10}Te_3$ at different temperatures.

Figure 3.4 shows the magnetic field variation of Hall resistivity at different temperatures for $Sb_{1.90}Cu_{0.10}Te_3$. We can easily observe three features from ρ_{xy} vs. B graph: (i) background is linear at large field, (ii) it is non-linear at low field, (iii) it switches its sign from positive to negative before reaching at zero field. Linearity in the graph clearly indicates the ordinary Hall effect (OHE) whereas presence of multicarrier and anomalous Hall effect (AHE) may be two responsible factors for the non-linearity in the Hall graph [shown in figure 3.4]. We have tried to fit the data by two band model but the extracted parameters were not feasible (not shown here), therefore, multicarrier contribution can be excluded easily. Hence, one can conclude that AHE is the responsible factor for the nonlinearity in the graph at low field. Presence of AHE is also an indication of magnetic ordering [63]. Moreover, Hall resistivity is switching sign from positive to negative at low field before reaching the zero value indicating the presence of topological Hall effect (THE) [55]. Hence, total Hall resistivity may be expressed as the combination of three terms OHE, AHE and THE.

$$\rho_{xy} = R_o H + R_s M + \rho^{TH} \tag{3.2}$$

Here ρ_{xy} is the total Hall resistivity. R_0 and R_s are respectively the OHE and AHE coefficients and M is the out of plane magnetization. Third term represents the topological Hall Effect. The coefficient of anomalous Hall effect (AHE) can be represented as

$$R_s = a\rho_{xx} + b\rho_{xx}^2 \tag{3.3}$$

The linear and quadratic terms indicate respectively, the skew scattering and scattering independent contribution to Hall resistivity. However, in consistent with the previous report the linear term can be neglected [64], [65]. Topological Hall effect is absent ($\rho^{TH} = 0$) at

high magnetic field. It is observed that at higher field when $\rho^{TH} = 0$, equation (2) can be simplified as

$$\frac{\rho_{xy}}{B} = R_o + \frac{b\rho_{xx}^2 M}{B} \tag{3.4}$$

If we linearly fit the $\frac{\rho_{xy}}{B}$ vs $\frac{b\rho_{xx}^2 M}{B}$ graph at the high magnetic field we can extract R_0 and b from the intercept and the slope of the curve respectively. We obtained a very good fit at high magnetic field with the fitting parameters R_0 and b as shown in figure 3.5 (a-d). Subtracting ordinary Hall resistivity ($R_o B$) and anomalous Hall resistivity ($b\rho_{xx}^2 M$) from the total Hall resistivity (ρ_{xy}) data in the full range of magnetic field, topological Hall resistivity (ρ^{TH}) has been extracted.

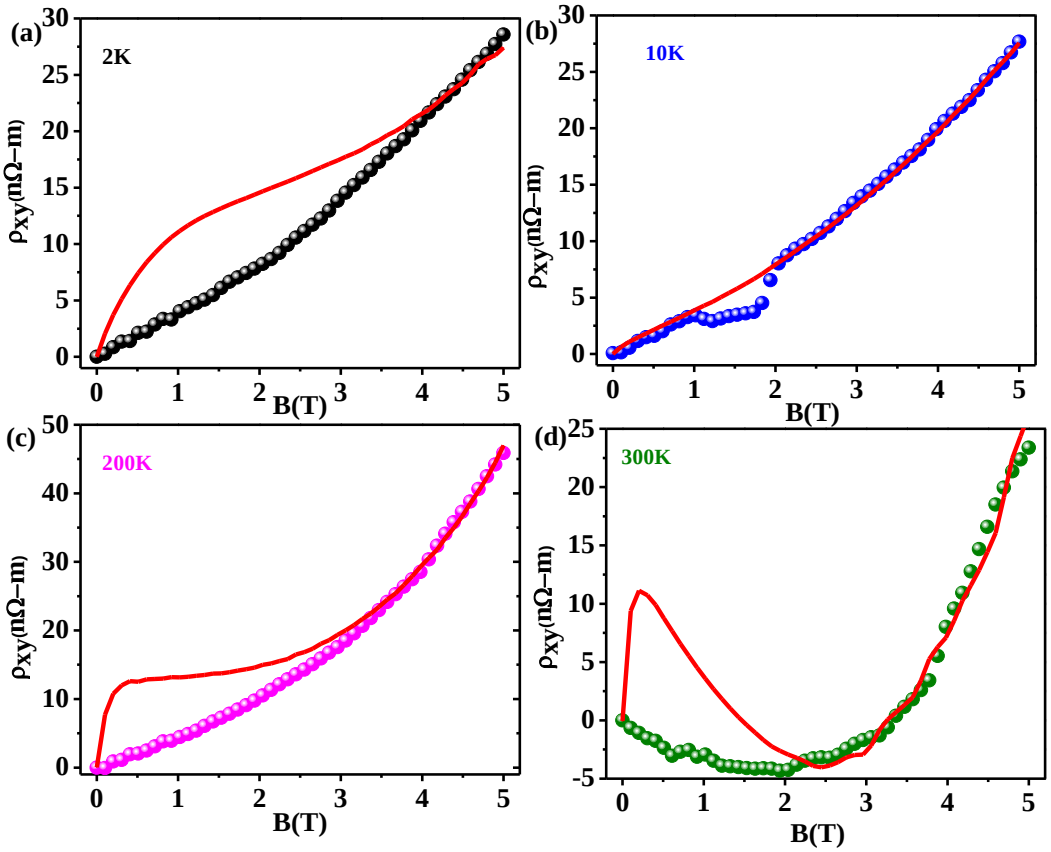

Figure 3.5: (a), (b), (c) and (d) The fitted Hall resistivity (ρ_{xy}) using the relation $\rho_{xy} = R_0B + b\rho_{xx}^2M$ at temperatures 2 K, 10 K, 200 K, 300 K respectively.

In fact, the signature of the existence of THE is observed at very low temperature (2 K) and at 300 K at a very low field (~0.25 T) it shows a maximum value (figure 3.6 (a)). Gallagher et al. and Yu et al. have shown that THE increases with increasing temperature [52]. The maximum reported temperature at which THE observed was 275 K [66]. But in the present investigation signature of THE is found even at room temperature. Moreover, the obtained topological Hall effect is as large as 1200 nΩ-cm which is even higher than the earlier reported values [55], [67], [68]. The highest reported value for THE was 1800 nΩ–cm which was obtained at very low temperature i.e. 2.5 K [18].

To investigate the origin of antiferromagnetism and to collect the information about the valence state and chemical bonding of the elements present in the lattice, we have used X-ray photoemission spectroscopy. The spectra of sample were taken from fresh surfaces prepared at room temperature (RT). Ar ion sputtering has been used to remove oxygen and carbon contamination. We have calibrated binding energies using C1s reference (284.2 eV). No other metal ions other than Sb, Cu and Te can be detected in the sample which clearly indicates that the prepared crystal is pure which is also consistent with XRD result. The experimental data were fitted by using XPS peak fit software. Figure 3.6 (I) is a typical low-resolution wide scan XPS spectra for the sample $Sb_{1.90}Cu_{0.10}Te_3$ showing the presence of elements Sb, Cu and Te in the sample. Figure 3.6 (II, III and IV) show the high resolution core level XPS spectra of Sb3d, Te3d and Cu2p respectively. Red lines are showing fitted data corresponding to spin states 3/2 and 1/2. Two peaks at 527.6 eV and 537.05 eV are observed in high resolution scan of the Sb3d region which corresponds to the binding energies of $Sb3d^{5/2}$ and $Sb3d^{3/2}$ spin states, respectively. These are also consistent with the reported data [69], [70]. Similarly two 3d Te spectral peaks corresponding to the

states of Te $3d^{5/2}$ and $3d^{3/2}$ at 571.6 and 582.02 respectively, also well matched with the observed data [69], [70]. Figure 3.6 (IV) shows the high resolution XPS spectra of Cu2p levels in doped sample. Two peaks at 931.6 eV and 949.8 eV reveal the $Cu2p^{3/2}$ and $Cu2p^{1/2}$ states respectively. The peak at 945.2 eV has been attributed to the satellites peaks of Cu2p. The satellite peak corresponds to the 945.2 eV is a clear indication of Cu^{2+} spin state [71]–[74]. People claimed that Cu^{2+} state is magnetic since $3d^9$ configurations have unpaired electrons [75]–[79]. It is observed from the analysis of the data that Cu is in Cu^{2+} state which might be a reason for the origin of antiferromagnetic ordering in the present investigation.

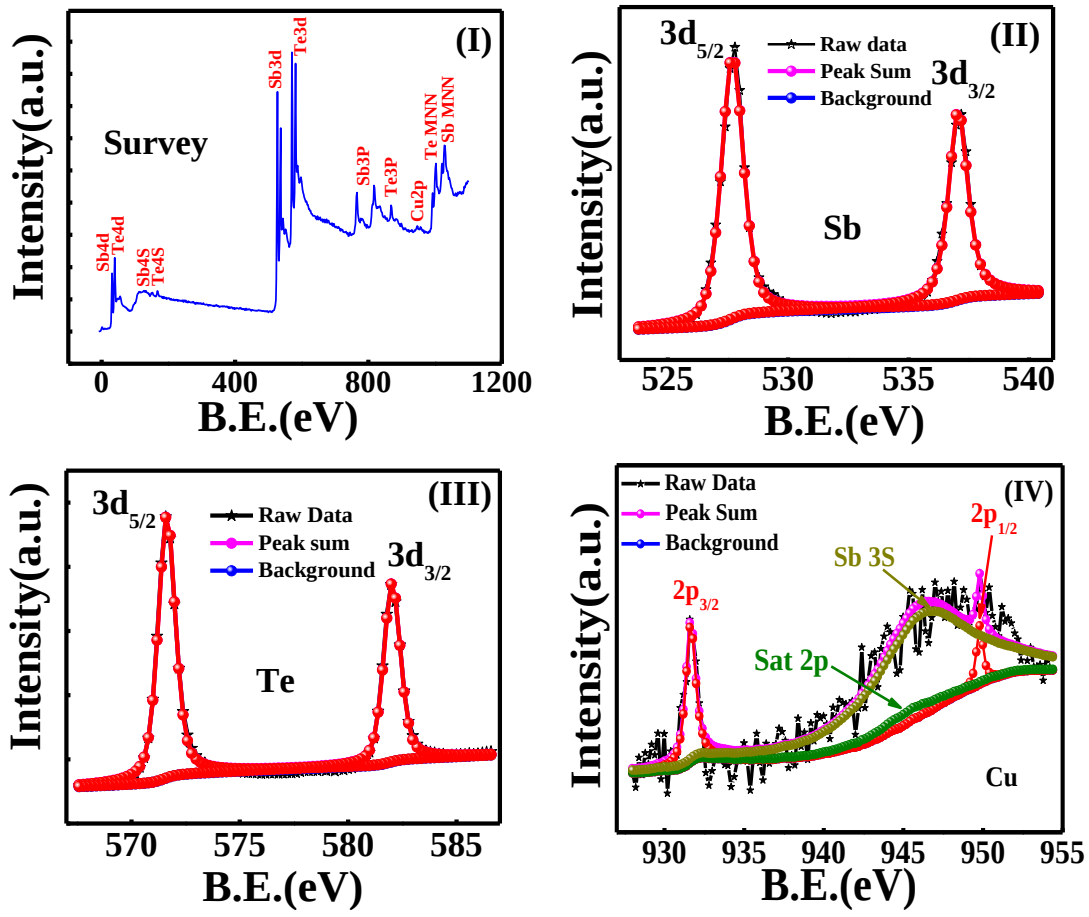

Figure 3.6: (I) X-ray Photoemission full survey spectrum of $Sb_{1.90}Cu_{0.10}Te_3$ (II), (III) & (IV): X-ray Photoemission core level spectrum of Sb, Te and Cu in $Sb_{1.90}Cu_{0.10}Te_3$ sample respectively.

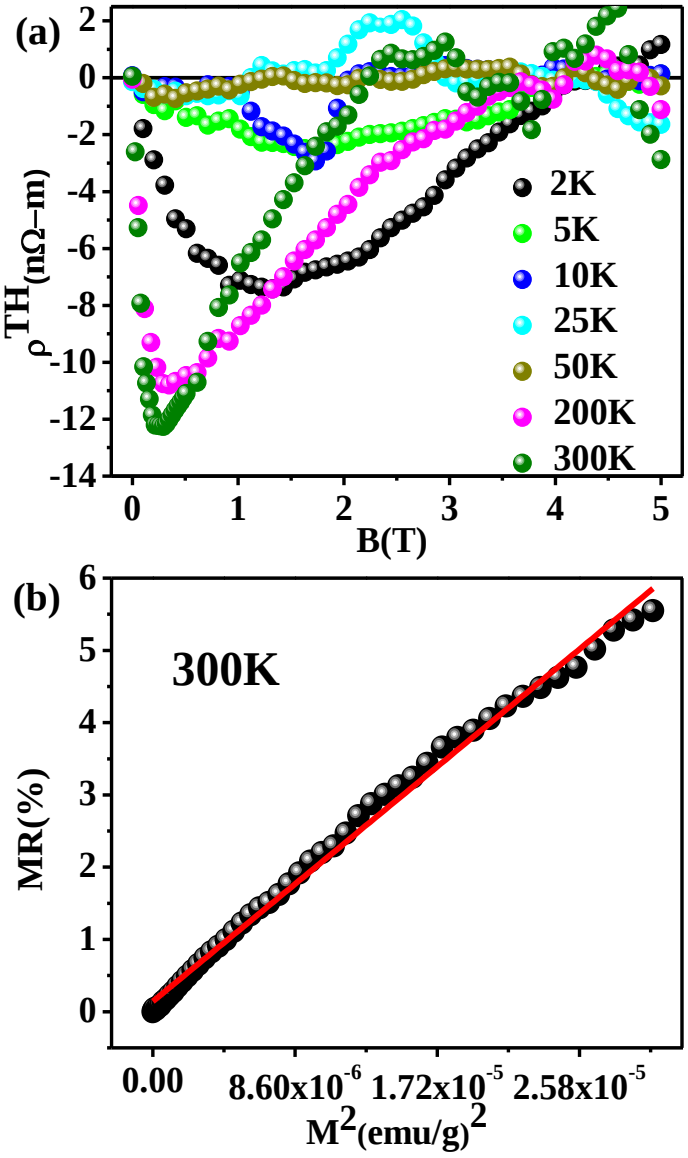

Figure 3.7: (a) Topological Hall effect (ρ^{TH}) at different temperatures as a function of magnetic field. (b) Linear fit of MR vs. M^2.

In fact, spin texture is the origin of THE [80], [81]. Linear fit of MR vs. M^2 (shown in figure 3.7(b)) is clearly indicating the presence of spin texture in $Sb_{1.90}Cu_{0.10}Te_3$ which is also consistent with M (B) and M (T) analysis showing magnetic ordering. It is also clear from XPS analysis that Cu is in +2 states i.e. $3d^9$ states, hence it should contain one unpaired electron and the corresponding magnetic moment for this state should be $\sqrt{3}$ Bohr magneton. The spins are in anti-parallel alignment which gives rise to antiferromagnetic

state. Moreover, from the above discussion it is clear even with the Cu doping the strong spin-orbit coupling exists in this Cu doped Sb_2Te_3.

Recently, in antiferromagnets, theoretically it is observed that a band structure induced THE might be due to the presence of non-collinear spin structure which breaks both the time reversal and lattice symmetries [60], [82]. Such a situation is observed in the present system as the AFM spins cant at finite magnetic field. Magnetic data support both the AFM ordering and a FM canting as is evident by an increase in magnetization with field and existence of hysteresis loop (Figure 3.3 Inset). As a matter of fact, in an AFM system with such broken time-reversal symmetry and spin-orbit coupling the THE is predicted to be significant.

3.3.2 Theoretical Study

In order to unearth underlying physics of Cu doped Sb_2Te_3, we have also carried out first principle calculation using full potential linear Augmented Plane wave (FP-LAPW) method which is popularly known as WIEN2k [83]. The exchange correlation effects are treated within local spin density approximation (LSDA) for spin polarized case [84] within the density function theory [85]. In the present calculations, the sphere radii of Cu, Sb and Te are chosen to 2.25, 2.28 and 2.28 a.u., respectively. Within these spheres, the charge density and potential are expanded in terms of crystal harmonics. The value of $K_{max} \times R_{MT} = 7.0$ (where R_{MT} and K_{max} are the atomic sphere radii and interstitial plane wave cut off), $G_{max=}14$ and $l_{max}=10$ are used for charge density Fourier expansion and wave function expansions inside the sphere. We use 181 k-points in the irreducible BZ to calculate electronic and magnetic properties of Cu doped Sb_2Te_3. We have considered measured value of the lattice constants (a = 4.25 Å and c = 30.4 Å) for all sets of calculation and the

atomic positions are relaxed. However, the optimized value between any two quintuple layers (QL) equal to 2.76 Å has been used throughout the calculation. Some general features of the relaxation are noted that the Cu atom replace Sb which lies between two Te atoms. While relaxation of the atomic positions the neighboring atoms move to accommodate the smaller radius of the Te atoms, the rest of the atoms show small changes in order to maintain the original crystal structure.

We have performed detail calculation for all the three magnetic phases of Cu doped Sb_2Te_3 i.e., paramagnetic (PM), ferromagnetic (FM), antiferromagnetic (AFM) phases. The calculated total energy/atom with spin orbit coupling (SOC) for PM, FM and AFM states are respectively, -12699.372906, -12699.379561 and -12699.381522 Ry/atom. The minimum value of total energy/atom is suggesting that AFM phase is the most stable state. The FM state shows very feeble magnetic moment of $2x10^{-5}$ ($3.2467x10^{-1}$) μ_B without (with) SOC. Further, in order to confirm the stable AFM state, we have performed detail electronic structure calculation. The relaxed unit cell of Sb_5CuTe_9 is shown in figure 3.8 (a). This is important to mention that while doing calculation for AFM state we took supercell of 30 atoms. Nevertheless, the concentration of Cu in Sb_5CuTe_9 is much higher than experimental realization; therefore, calculations are performed at this concentration to understand the Cu-d states and stability of different phases. The theoretical calculation supports our experimental observation.

The calculated band structure of Sb_5CuTe_9 with SOC for the AFM phase and corresponding first Brillouin Zone (BZ) are presented in figure 3.8 (a). The band structure shows very narrow band gap at the centre of BZ (Gamma) and the Fermi level lies ~140meV below the centre of gap, supports p- type nature of the sample (Inset of figure 3.8

(b)). Further in order to see the energy band gap in between valence band maxima (VBM) and conduction band minima (CBM), we have magnified the band structure in the energy range between -1.0 to 1.0 eV as presented in the right inset of the figure 3.8 (b). The CBM is mainly composed of Sb-p and Cu-d with a small contribution from Te-p. The total density of states presented along with band structure shows strong peak near ~ -2.1 eV corresponding to Cu-d states. On the other hand, VBM is composed of mainly Cu-d orbital with the strong hybridization from Te-p orbital. The layered structure of Sb_5CuTe_9 and size mismatch between Cu and Sb/Te site weaken the hybridization fairly by replacing Sb by Cu. The total density of states (TDOS) for of Sb_5CuTe_9 is presented in figure 3.8 (b). The calculated TDOS shows strong peak just below the VBM (~ -2.1 eV) appearing mainly from Cu-d. At the VBM there is strong hybridization between Cu-d and Te-p states (~ -0.65 eV). On the other hand, Sb-p states are dominated in the CBM with a considerable contribution from Te-p. Moreover, Cu-d state shows strong hybridization with Sb-p and Te-p at ~2.6 eV. Overall near the VBM Cu-d is dominant while CBM is dominated by Sb-p and Te-p shows strong hybridization between them.

However, we have discussed above spin texture as the origin of the THE in Cu-doped Sb_2Te_3 at finite magnetic field as is observed in FM system [54], [55], [81], if driven to anti-crossings near Fermi level. It is also clear from figure 3.8 (b) that with Cu doping anti-crossing at Fermi level is observed. This may carry the significant Berry curvature. The large spin-orbit coupling along with the critical band alignment may enhance the effect of the Cu spin texture on these bands. Therefore, significant Berry phase contributes to the THE due to the development of spin-texture with the evolution of electronic structure.

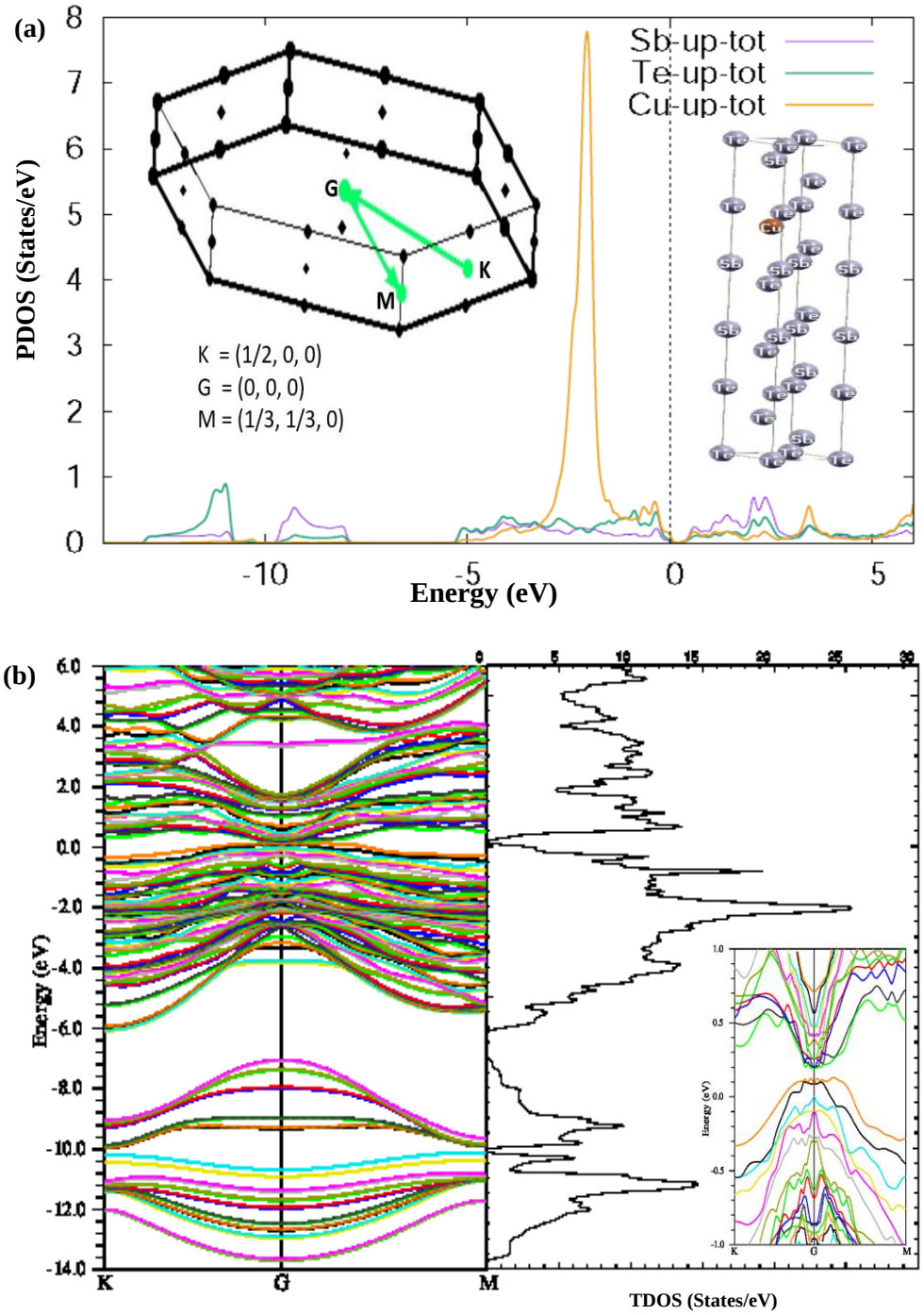

Figure 3.8: (a) Calculated projected density of states (PDOS) for Cu, Sb and Te. Right Inset: The crystal structure of Sb_5CuTe_9. The five atoms "quintuple layer leaves" are separated by a van der walls gap equal to 2.76 Å. Different colors of the spheres are marked with corresponding element symbol. Left Inset: First BZ of Sb_5CuTe_9 and along selected path corresponding to dispersion curve. (b) Calculated band structure along M G and K direction for Sb_5CuTe_9, Calculated total density of states (TDOS) for Sb_5CuTe_9. Inset: Magnified view at Gamma point.

3.4 Conclusion

In conclusion, Hall data indicate the existence of anomalous and topological Hall effects even at room temperature. Magnetization data indicates that the Cu doped Sb_2Te_3 is in the AFM state. But with application of magnetic field the spin structure cants ferromagnetically which is observed from the appearance of hysteresis loop in M (B) curve. The observed THE might be due to the spin textures which is clear from the linear variation of MR with M^2. The band structure confirms the existence of spin texture. We have measured the magnetotransport and magnetization at different temperatures and different fields. We find the coexistence of both bulk and surface states from the quantum oscillations. The observed room temperature antiferromagnetism is due to the Cu^{2+} spin state. Moreover, THE has been established at room temperature which may be very promising for the spintronic devices working at room temperature.